Acta Crystallographica Section D
Biological Crystallography
ISSN 0907-4449

High-resolution neutron structure of nicotinamide adenine dinucleotide

Benoit Guillot,[a] Claude Lecomte,[a] Alain Cousson,[b] Christian Scherf[b,c] and Christian Jelsch[a]*

[a]Laboratoire de Cristallographie et de Modélisation des Matériaux Minéraux et Biologiques (LCM^{3}B), CNRS ESA 7036, UHP Faculté des Sciences, BP 239, 54506 Vandoeuvre-les-Nancy CEDEX, France, [b]Laboratoire Léon Brillouin (CEA–CNRS), CEA Saclay, 91191 Gif-sur-Yvette CEDEX, France, and [c]Institut für Kristallographie, RWTH Aachen, 52056 Aachen, Germany

Correspondence e-mail: jelsch@lcm3b.uhp-nancy.fr

Received 26 February 2001
Accepted 27 April 2001

NDB Reference: NAD$^+$, ur0013.

The structure of the free-acid form of the coenzyme NAD$^+$ was determined at 100 K from a single-crystal neutron experiment. NAD$^+$ is the oxidized form of the coenzyme redox pair NAD$^+$/NADH and plays an important role in the catalysis of biological processes. The molecule crystallizes in space group $P1$ with one NAD$^+$ and four water molecules per unit cell. The structure is compared with the previous X-ray models of NAD$^+$ [Reddy *et al.* (1981), *J. Am. Chem. Soc.* **103**, 907–914; Parthasarathy & Fridey (1984*b*), *Science*, **226**, 969–971; Guillot *et al.* (2000), *Acta Cryst.* C**56**, 726–728]. The crystal packing and the hydrogen-bond pattern are discussed as well as four short C—H···O contacts involving the pyridine and adenine rings. The structure displays stereochemical distortions owing to the hydrogen bonding and crystal-packing constraints, reflecting the adaptability of the NAD$^+$ molecule in various chemical environments.

1. Introduction

The nicotinamide adenine dinucleotide cofactor (NAD$^+$) plays a major role in enzyme-catalyzed biological oxido-reduction processes. NAD$^+$ is the oxidized form of the redox pair NAD$^+$/NADH and binds to enzymes involved in catabolic oxidative reactions, mostly dehydrogenases. As depicted in Fig. 1, the NAD$^+$ molecule is composed of a pyrophosphate moiety linking an adenylic acid and a nicotinamide-5′-ribonucleotide group together. In the dehydrogenation process, the NAD$^+$ molecule is reduced to NADH by accepting a hydride anion (H^+, $2e^-$) from the substrate to its redox-active site located on the C18 atom (in the present paper nomenclature) of the nicotinamide ring. The goal of this study was to determine accurately the position of the protons of the molecule as well as their anisotropic thermal displacement parameters, to be used in a further $[X - (X + N)]$ charge-density analysis. This structure is described and compared with the X-ray structure recently deposited at the Cambridge Structural Database (Guillot *et al.*, 2000) and to the lithium dihydrate complex of NAD$^+$ (Saenger *et al.*, 1977; Reddy *et al.*, 1981).

2. Experimental

2.1. Crystallization

NAD$^+$ was purchased in lyophilized form from Sigma (St Louis, USA). The crystallization solution was prepared in the following way: 1 g of NAD$^+$ was dissolved in 1 ml purified water. 50 µl LiOH (1 *M*) was then added to 100 µl of the solution. Finally, 200 µl methanol was slowly added to reduce the solubility of NAD$^+$. The pH of the final solution was about

Table 1
Crystallographic data.

Radiation type	Neutron
Wavelength (Å)	0.8305 (2)
Space group	Triclinic *P*1
Z	1
F(000) (e)	384
Unit-cell parameters	
a (Å)	8.57 (1)
b (Å)	8.83 (1)
c (Å)	11.19 (1)
α (°)	109.7 (1)
β (°)	90.6 (1)
γ (°)	104.0 (1)
Resolution (Å)	0.65 ($-13 \le h \le 13$, $-13 \le k \le 13$, $-17 \le l \le 1$)
No. of measured reflections	6343
No. of unique reflections	5990
No. of reflections with $I/\sigma(I) > 3$	4988
$R_{\rm merge}(I)$†	0.056
$\langle I/\sigma(I)\rangle$	
All reflections	12.9
Highest resolution, $d < 0.67$ Å	6.5
Reflections with $I/\sigma(I) > 3$ (%)	
All reflections	78
Highest resolution, $d < 0.67$ Å	61
R (F)‡	
All reflections	0.095
$I/\sigma(I) > 3$	0.062
wR (F)§	
All reflections	0.054
$I/\sigma(I) > 3$	0.050
GoF¶	
All reflections	1.95
$I/\sigma(I) > 3$	2.00

† $R_{\rm merge}(I) = \{\sum_{\mathbf{h}} \sum_i [w_{\mathbf{h},i}(I_{\mathbf{h},i} - \langle I_{\mathbf{h}}\rangle)^2]/(\sum_{\mathbf{h}} \sum_i w_{\mathbf{h},i}\langle I_{\mathbf{h},i}\rangle^2)\}^{1/2}$. ‡ $R(F) = \{\sum_{\mathbf{h}}[|F_{\rm obs}(\mathbf{h})| - |F_{\rm calc}(\mathbf{h})|]^2/\sum_{\mathbf{h}}|F_{\rm obs}(\mathbf{h})|^2\}^{1/2}$. § $\mathrm{wR}(F) = \{\sum_{\mathbf{h}} w[|F_{\rm obs}(\mathbf{h})| - |F_{\rm calc}(\mathbf{h})|]^2/\sum_{\mathbf{h}} w|F_{\rm obs}(\mathbf{h})|^2\}^{1/2}$. ¶ $\mathrm{GoF} = \{\sum_{\mathbf{h}} w[|F_{\rm obs}(\mathbf{h})| - |F_{\rm calc}(\mathbf{h})|]^2/(N_{\rm obs} - N_{\rm par})\}^{1/2}$. $w_{\mathbf{h},i} = 1/\sigma(I_{\mathbf{h},i})^2$ is the weighting factor for observation number i of the reflection $\mathbf{h}$. $w = 1/\sigma_F^2$ is the weighting factor of the unique reflection $\mathbf{h}$. $N_{\rm obs}$ is the number of observations used for the refinement and $N_{\rm par}$ the number of refined parameters; $F_{\rm obs}$ are the *scaled* observed structure-factor amplitudes and $F_{\rm calc}$ the calculated structure-factor amplitudes.

3.5. Several identical batches were prepared, with crystals appearing in all of them after 48 h. One of the batches contained a 5.5 × 1.4 × 1.3 mm colourless crystal suitable for a neutron-diffraction experiment.

2.2. Data collection

The neutron-diffraction data were collected at cryogenic temperature [100 (2) K] with a Stoe four-circle diffractometer on the 5C2 channel at the Léon–Brillouin Laboratory facility (CNRS-CEA, Saclay, France). The 5C2 channel is at the end of a neutron hot-source line [λ = 0.8305 (2) Å] at the ORPHEE reactor. The diffractometer was equipped with a Cu(220) monochromator and an Oxford Instruments helium vapour-stream cryostat. Because of the relatively small size of the crystal for this type of experiment, 20 d exposure were necessary to collect a hemisphere of data. NAD^+ crystals decay after long exposure to air. To protect it, the crystal was mounted in aluminium foil and placed in a helium atmosphere. The lattice parameters were obtained by a least-squares fit using 12 reflections within the $32.2 < 2\theta < 39.7°$ angular range. During the data collection, a standard reflection (−2, −2, −5) was measured at 7.5 h intervals and showed no detectable decay. The data were corrected for Lorentz effects but not for absorption ($\mu_{\rm est}$ = 0.18 mm^{-1}) as the crystal was of small size and cylindrical shape. The Friedel pairs were not averaged but an internal agreement factor calculated on the 353 measured Friedel equivalent reflections leads to $R_{\rm merge}$ = 0.056.

2.3. Neutron least-squares refinement

The initial coordinates were taken from the X-ray structure of NAD^+ (Guillot *et al.*, 2000) and refined against the neutron-diffraction data [$I > 3\sigma(I)$] using the program *MOPRO* (Guillot *et al.*, 2001). The refinement was performed against the structure-factor moduli $|F|$, with a weighting scheme $w = 1/\sigma_F^2$. Data-collection and refinement statistics are given in Table 1. During the refinement, all the atoms were refined anisotropically without application of any restraint. There were 249 positional and 498 thermal displacement refined parameters, leading to a ratio of observations to variables of 6.7. To refine the structure, the following refinement strategy was applied: first, all the thermal motion parameters and the positions of all atoms except O1 were refined separately. The positional and thermal motion parameters of all atoms of the nicotinamide ribonucleotide were then refined together, the other atoms remaining fixed. The same procedure was applied to the atoms of the adenine side of the molecule and finally to the atoms of the pyrophosphate group. This method avoids the problem of the floating origin in space group *P*1, as some heavy-atom coordinates are kept fixed during each stage of the refinement. The whole procedure was cycled until total convergence, then a final full normal matrix inversion with all the atomic parameters except the O1 coordinates was performed to extract the standard uncertainties, parameter correlation and to calculate the goodness of fit (S). At the end of the refinement, the statistical agreement factor R_w was 5.04% for reflections with $I > 3\sigma(I)$. The extinction (Lorenz, type I) was found to be very small, with a maximal value y = 0.917 for the $(\bar{2}00)$ reflection.

3. Results and discussion

3.1. Comparison between neutron and X-ray structures

A view of the molecule with the atomic thermal ellipsoids is shown in Fig. 2. The distances between bonded atoms in NAD^+ are given in Table 2 and selected torsion and angle values in Table 3. The discrepancy of the covalent bond

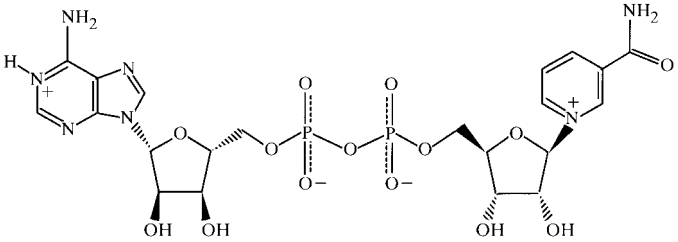

Figure 1
Chemical structure of the NAD^+ molecule. The H atoms linked to C atoms have been omitted.

lengths in the NAD^+ X-ray (Guillot *et al.*, 2000) and neutron structures is illustrated in Fig. 3. The root-mean-square (r.m.s.) coordinate difference between the two structures, excluding H atoms, is 0.04 Å. All the torsion, angle and planarity values are similar within standard uncertainties, but the comparison between bond lengths involving non-H atoms reveals interesting features. The shortening of the neutron bond lengths compared with the X-ray bond lengths represents the most significant difference. Interestingly, this shortening is more pronounced for the bonds involving an O atom [average discrepancy $\langle (D_X - D_N)/D_N \rangle = 0.4\%$], while the C—N bonds and the C—C bonds are less affected (average discrepancy of 0.25 and 0.07%, respectively).

One could explain this particular feature by the fact that the O-atom lone pairs are localizable in the electron density at the resolution of the X-ray experiment (0.6 Å), but are not modelled by the spherical atom model (Hansen & Coppens, 1978; Jelsch *et al.*, 1998). This results in a slight overestimation of some bond lengths in the X-ray structure, as the O atom may be slightly pulled in the direction of the non-modelled lone pairs. To check this hypothesis, an X-ray high-order refinement ($0.7 < d < 0.6$ Å) of the NAD^+ structure has been performed. This refinement is less sensitive to the valence density of the atoms and, as expected, leads to systematically shorter X—O bond lengths, closer to the neutron values (Fig. 3; Dunitz & Seiler, 1973). The X—O bond lengths from the X-ray high-order refinement are only 0.2% longer on average compared with the bonds from the neutron experiment. For the C—N and C—C bond, the average lengthening after the high-order refinement is 0.14 and 0.1%, respectively. Thus, a global positive discrepancy remains even for the high-order X-ray refinement as also suggested by examination of Fig. 3. This bond-length discrepancy may be attributed to the disagreement between X-ray and neutron unit-cell parameters (§3.2). To test this hypothesis, a high-order X-ray refinement (at resolution $d < 0.65$ Å) has been performed using the neutron unit-cell parameters. The disparities between bond lengths at the end of this refinement are uniformly and symmetrically distributed within 1.5σ (average of 0.1, 0.06 and −0.01% for X—O, C—N and C—C bonds, respectively). Hence, the observed discrepancies between X-ray and neutron bond lengths are a consequence of both the contribution of the unit-cell parameters shortening (0.16% on average) and of the non-modelled electron doublets of O and N atoms.

Table 2
Bond lengths (Å).

P1—O2	1.486 (5)	C3—O6	1.423 (5)
P1—O3	1.501 (5)	C3—C4	1.538 (5)
P1—O4	1.597 (6)	C4—O7	1.396 (5)
P2—O8	1.476 (5)	C4—C5	1.545 (5)
P2—O9	1.485 (6)	C5—O5	1.398 (5)
P2—O10	1.596 (5)	C11—O10	1.435 (5)
P1—O1	1.580 (5)	C11—C12	1.506 (5)
P2—O1	1.621 (5)	C12—O11	1.453 (5)
C1—O4	1.451 (5)	C12—C13	1.537 (5)
C1—C2	1.505 (5)	C13—O12	1.410 (5)
C2—O5	1.445 (5)	C13—C14	1.531 (5)
C2—C3	1.523 (4)	C14—O13	1.417 (5)
C14—C15	1.536 (5)	C15—O11	1.381 (5)
N4—C10	1.324 (4)	C5—N1	1.457 (4)
C15—N6	1.496 (4)	N1—C6	1.363 (4)
N6—C20	1.346 (4)	N1—C10	1.371 (4)
N6—C16	1.347 (4)	C6—N2	1.349 (4)
C16—C17	1.379 (5)	C6—C9	1.390 (4)
C17—C18	1.384 (5)	N2—C7	1.316 (4)
C18—C19	1.398 (5)	C7—N3	1.353 (4)
C19—C20	1.391 (5)	N3—C8	1.368 (4)
C19—C21	1.500 (5)	C8—N5	1.314 (4)
C21—O14	1.233 (5)	C8—C9	1.415 (5)
C21—N7	1.335 (4)	C9—N4	1.372 (4)
C1—HC1A	1.081 (8)	C7—HC7	1.101 (8)
C1—HC1B	1.087 (8)	N3—HN3	1.097 (7)
C11—H11A	1.089 (9)	C10—HC10	1.085 (8)
C11—H11B	1.078 (9)	N7—HN7A	1.036 (8)
O6—HO6	1.012 (7)	N7—HN7B	1.031 (7)
O7—HO7	0.984 (7)	C16—HC16	1.091 (8)
O12—HO12	0.987 (8)	C17—HC17	1.092 (8)
O13—HO13	0.987 (9)	C18—HC18	1.103 (8)
C2—HC2	1.093 (7)	C20—HC20	1.077 (7)
C3—HC3	1.099 (7)		
C4—HC4	1.109 (7)	OW1—HW1A	0.975 (8)
C5—HC5	1.113 (7)	OW1—HW1B	0.969 (9)
C12—HC12	1.108 (7)	OW2—HW2A	0.973 (9)
C13—HC13	1.094 (8)	OW2—HW2B	0.995 (9)
C14—HC14	1.105 (8)	OW3—HW3A	0.963 (9)
C15—HC15	1.108 (7)	OW3—HW3B	0.965 (9)
N5—HN5A	1.040 (7)	OW4—HW4A	0.97 (1)
N5—HN5B	1.027 (7)	OW4—HW4B	0.95 (1)

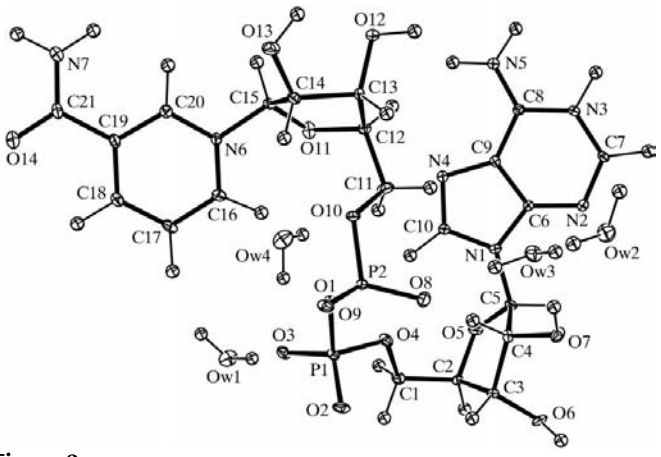

Figure 2
*ORTEP*III view of the NAD^+ molecule and the water molecules (Burnett & Johnson, 1996; Farrugia, 1997). Thermal ellipsoids are at the 50% probability level for all atoms.

3.2. Thermal motion

The unit-cell parameters refined against the neutron data are slightly different from those found using X-rays. The unit-cell volumes are 773.7 (14) Å^3 for the X-ray and 769.9 (14) Å^3 for the neutron experiments, possibly owing to different data collection temperatures. This is confirmed by a poor agreement between the neutron and X-ray thermal parameters. The equivalent isotropic U_{eq} thermal factors of the non-H atoms of the present structure have been plotted on Fig. 4 *versus* those of the X-ray structure. The equivalent thermal factors U_{eq}(X-ray) and U_{eq}(neutron) (of the non-H atoms) are proportional with a ratio of 1.16 (7) (Coppens & Vos, 1971). The temperature of the neutron experiment is more reliable

Table 3
Selected bond and dihedral angles (°).

Angles (°).

P1—O1—P2	132.0 (3)	O8—P2—O9	120.3 (3)
O2—P1—O3	115.3 (3)	O8—P2—O10	110.9 (3)
O2—P1—O1	112.8 (3)	O9—P2—O10	106.8 (3)
O3—P1—O1	106.8 (3)	O8—P2—O1	109.8 (3)
O2—P1—O4	110.6 (3)	O9—P2—O1	108.3 (3)
O3—P1—O4	109.9 (3)	O10—P2—O1	98.5 (3)
O1—P1—O4	100.5 (3)	C11—O10—P2	116.1 (3)
C1—O4—P1	115.7 (3)	O10—C11—C12	108.4 (3)
O4—C1—C2	109.2 (3)	O14—C21—N7	122.9 (3)

Dihedral angles (°).

P2—O1—P1—O4	−84.0 (4)
P1—O4—C1—C2	−147.1 (3)
O1—P1—O4—C1	−176.9 (3)
O5—C5—N1—C10	34.2 (4)
C18—C19—C21—O14	12.4 (5)
P1—O1—P2—O10	160.9 (3)
P2—O10—C11—C12	170.1 (3)
O1—P2—O10—C11	−70.9 (4)
O11—C15—N6—C20	−150.2 (3)
C20—C19—C21—N7	8.1 (5)

than the X-ray experiment, as the former was performed with a cryostat and the latter with a nitrogen-stream cooling device. Thus, if the equivalent isotropic B factor is supposed to vary linearly with the temperature, the temperature for the X-ray experiment can be estimated to be about 116 K. An interesting feature of the NAD^+ neutron model is the good result of the rigid-bond test (Hirshfeld, 1976). The average rigid-bond value for bonds involving non-H atoms is $\langle\Delta\rangle = 0.0012\ (10)$ Å^2 and $\langle\Delta\rangle = 0.0057\ (33)$ Å^2 for X—H bonds. These average values are of the same order of magnitude as the standard uncertainties of the anisotropic thermal displacement parameters and can then be a significant criterion to assess the quality of the thermal motion modelling. The largest discrepancy for bonds between non-H atoms is Δ = 0.00375 Å^2 for the P1—O2 bond. The largest discrepancy for bonds involving H atoms is for the OW4—HW4(A,B) bonds, which is consistent with the W4 water molecule atoms having the largest thermal motion in the whole structure.

3.3. NAD^+ structure and bond lengths

The folding of NAD^+ in its triclinic form is more compact than that found in holoenzyme complexes, where the molecule usually exhibits an extended shape. The conformation of the ribonucleotides composing the NAD^+ molecule in terms of nucleic acid terminology has already been extensively reported by Parthasarathy & Fridey (1984) in their room-temperature study and is not discussed here. If the differences between the two base rings are neglected, there is a pseudo-dyad axis passing through the middle of the pyrophosphate moiety relating the two nucleotides (Fig. 1). However, significant differences can be found between both sides of the molecule, especially for the bond lengths. There is a remarkable and still unexplained discrepancy between the P1—O1 = 1.580 (5) Å and P2—O1 = 1.621 (5) Å bond lengths (Table 2). This difference is, however, less pronounced in the neutron structure than in the X-ray model of NAD^+ (Guillot *et al.*, 2000) where the P2—O1 bond is even longer [d = 1.630 (2) Å].

In the study of the NAD^+Li^+ crystal structure, Saenger *et al.* (1977) reported a C15—N6 (1.55 Å) glycosidic bond which is 0.08 Å longer than the *a priori* equivalent C5—N1 bond (1.44 Å) between the ribose and the uncharged adenine. They attributed this feature to the positive charge located on the nicotinamide group. Furthermore, Miwa *et al.* (1999), in their charge-density study of the nicotinamide molecule, observed that the bonding electron density is stronger on the nicotinamide ring near the carboxamide moiety than around the N6 N atom. The weak C15—N6 bonding electron density correlates well with a lengthening of this bond. In the present structure, as the adenine carries also a positive charge, one

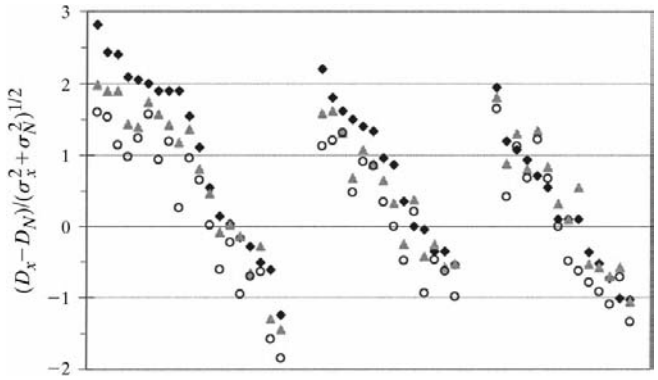

Figure 3
Bond-length discrepancies between the X-ray and neutron structures for O—X bonds (left), C—N bonds (middle) and C—C bonds (right). D_N stands for neutron-diffraction experiment bond lengths, D_X for X-ray bond lengths and σ_X and σ_N for X-ray and neutron standard deviations. D_X distances are taken from the conventional (black squares), high-order (grey triangles) and high order with neutron unit-cell parameters (open circles) X-ray refinements.

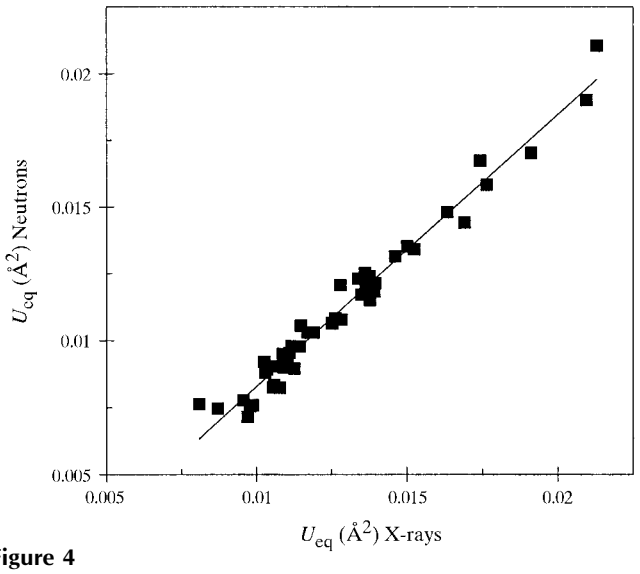

Figure 4
Equivalent isotropic thermal displacement parameters U_{eq} in the neutron structure (x axis) and in the high-order X-ray structure (y axis). $U_{eq} = \sum_i \sum_j U^{ij} a_i * a_j * \mathbf{a}_i \cdot \mathbf{a}_j / 3$.

Table 4
Lengths of the sugar–base joint bonds (glycosidic) and of the sugar ether bonds in selected high-resolution holoenzyme complexes, in the NAD^+Li^+ crystal and in the NAD^+ triclinic structure.

1bw9, phenylalanine dehydrogenase (Vanhooke *et al.*, 1999); 1ldg, L-lactate dehydrogenase (Dunn *et al.*, 1996); 1qrr, sulfolipid biosynthesis isomerase (Mullichak *et al.*, 1999); 1udb and 1udc, UDP-galactose-4-epimerase (Thoden, Hegeman *et al.*, 1997; Thoden, Gulick *et al.*, 1997); 3bto, alcohol dehydrogenase (Cho *et al.*, 1997); NAD^+Li^+ complex (Saenger *et al.*, 1977); X-ray NAD^+ (Guillot *et al.*, 2000).

		Glycosidic bonds (Å)		Ribose ether bonds (Å)			
PDB code	Resolution (Å)	C5—N1	C15—N6	C15—O11	C5—O5	O5—C2	O11—C12
1bw9 (dimer)	1.50	1.48	ND	ND	1.40	1.46	ND
		1.44	1.44	1.41	1.37	1.47	1.45
1ldg	1.75	1.47	1.48	1.43	1.42	1.43	1.44
1qrr	1.60	1.48	1.48	1.44	1.44	1.43	1.45
1udb	1.65	1.46	1.45	1.39	1.39	1.44	1.45
1udc	1.65	1.50	1.46	1.40	1.39	1.47	1.43
3bto (tetramer)	1.66	1.44	1.50	1.48	1.40	1.49	1.49
		1.43	1.51	1.44	1.40	1.50	1.50
		1.44	1.55	1.44	1.43	1.50	1.53
		1.45	1.54	1.44	1.43	1.49	1.53
Average		1.45 (2)	1.50 (4)	1.42 (3)	1.40 (2)	1.47 (3)	1.48 (4)
NAD^+Li^+	1.10	1.44	1.55	1.38	1.39	1.49	1.53
X-rays NAD^+	0.60	1.466	1.501	1.394	1.408	1.455	1.507
Neutron NAD^+	0.65	1.456	1.496	1.381	1.399	1.445	1.506

Table 5
Intermolecular interactions: distances and angles.

D—H···A interactions	D—H (Å)	A···H (Å)	D···A (Å)	D—H—A (°)
O6—HO6···N4^{ii}	1.005 (7)	1.825 (7)	2.770 (5)	153.9 (7)
O7—H7···OW3^{i}	0.984 (7)	1.722 (8)	2.693 (6)	168.2 (7)
O12—HO12···O14^{vi}	0.987 (8)	1.786 (9)	2.720 (7)	156.6 (7)
O13—HO13···O6^{vii}	0.987 (8)	2.076 (8)	2.903 (6)	140.1 (7)
N3—HN3···O2^{iii}	1.099 (7)	1.516 (8)	2.613 (5)	174.3 (8)
N5—HN5A···O3^{iv}	1.040 (7)	1.813 (8)	2.832 (6)	165.4 (7)
N5—HN5B···O7^{v}	1.027 (7)	1.856 (8)	2.828 (5)	156.6 (6)
N7—HN7A···OW2^{viii}	1.036 (8)	1.937 (9)	2.969 (6)	173.1 (7)
N7—HN7B···O9^{v}	1.031 (7)	1.780 (8)	2.808 (6)	173.6 (8)
OW1—HW1A···O3^{i}	0.975 (8)	1.831 (9)	2.787 (6)	165.6 (8)
OW1—HW1B···N2^{ix}	0.968 (9)	2.010 (9)	2.978 (6)	176.8 (8)
OW2—HW2A···OW1^{x}	0.973 (9)	1.838 (9)	2.809 (7)	175.2 (8)
OW2—HW2B···O6^{xi}	0.995 (9)	1.88 (1)	2.874 (7)	179.0 (9)
OW3—HW3A···OW2^{i}	0.963 (9)	1.984 (9)	2.937 (6)	169.7 (9)
OW3—HW3B···O8^{i}	0.965 (8)	1.806 (9)	2.745 (7)	163.6 (8)
OW4—HW4A···O3^{i}	0.97 (1)	1.92 (1)	2.891 (7)	171.4 (10)
OW4—HW4B···O13^{xii}	0.95 (1)	1.80 (1)	2.748 (7)	176.7 (10)

Symmetry codes: (i) x, y, z; (ii) $x, y-1, z$; (iii) $x, y+1, z+1$; (iv) $x, y+1, z+1$; (v) $x, y+1, z$; (vi) $x, y, z+1$; (vii) $x-1, y+1, z$; (viii) $x, y+1, z-1$; (ix) $x, y, z-1$; (x) $x-1, y, z+1$; (xi) $x-1, y, z$; (xii) $x+1, y, z$.

could expect a lengthening of the C5—N1 bond according to Saenger's hypothesis. However, the C5—N1 bond has a length of 1.456 Å, which is only 0.016 Å longer than in the NAD^+Li^+ structure. On the other hand, the C15—N6 bond is significantly shortened, with a length of 1.496 Å (Table 2), resulting in a smaller discrepancy between the two glycosidic C—N bonds.

The ether bonds of both ribose rings show a pronounced asymmetry. In the nicotinamide sugar the O11—C15 and O11—C12 bond lengths are 1.381 and 1.453 Å, respectively. The equivalent bonds of the adenine ribose also have dissimilar lengths of 1.397 and 1.445 Å. These distances are slightly different from those of the NAD^+ X-ray structure, for the reasons discussed in §3.1.

Again, the comparison of the ether and glycosidic bonds in the NAD^+ X-ray structure and the corresponding bonds in the NAD^+Li^+ complex reveals large discrepancies, even within the 0.02 Å estimated standard deviations (e.s.d.) of the 1.1 Å resolution lithium salt NAD^+ structure. To assess if the presence of positive charges on the adenine ring could be at the origin of such differences, all the NAD^+ molecules from the six holoenzyme complexes solved at more than 1.8 Å resolution present in the Protein Data Bank (Berman *et al.*, 2000) have been examined. The corresponding glycosidic and ribose C—O—C bond lengths are reported in Table 4.

It has to be remembered here that the e.s.d. on bond lengths in structures around 1.8 Å resolution is much higher (∼0.05 Å) and that the introduction of restraints during the refinement of the models necessarily has an influence on the refined bond lengths (Cruickshank, 1999). In the stereochemical dictionary file 'param.nad' used by the *X-PLOR* macromolecular structure-refinement program (Brünger, 1992), an identical restraint target is given for the two glycosidic bonds (d = 1.48 Å) as well as for the four ether bonds (d = 1.435 Å). Despite the identical restraint target used for the different types of bonds, several classes of bond lengths appear in Table 4 for both the ether and the glycosidic bonds in the NAD^+ protein cofactors. Each type of bond length has a variability between 0.02 and 0.04 Å in the sample of holoenzymes analyzed. The C5—O5 and C15—O11 ether bonds have generally similar lengths around 1.41 Å, while the C2—O5 and C12—O11 bonds have on average higher lengths around 1.48 Å. For the accurate refinement of NAD^+–holoenzyme complexes, it is therefore essential to assign specific target values for the different ether and glycosidic bond types of the cofactor.

The variability of the bond lengths in the NAD^+ molecule presumably reflects a global adaptability of the cofactor to its protein environment, probably related to complex electronic features which will be interesting to characterize in a charge-density study.

3.4. Crystal packing and hydrogen bonding

In the triclinic crystal form of the NAD^+ molecule, the adenine N3 atom is protonated owing to the acidity of the

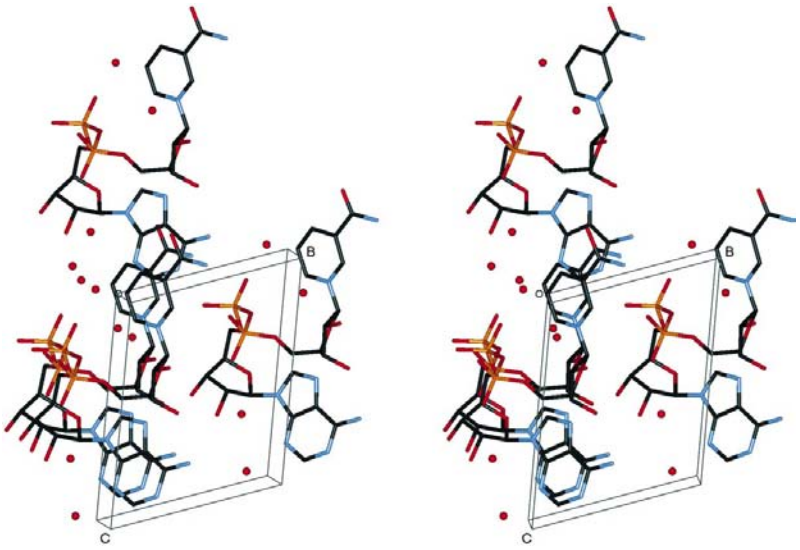

Figure 5
View of the NAD^+ crystal packing in projection along the *a* axis. The H atoms are omitted and the water molecules are displayed as spheres.

crystallization solution. This results in the global electroneutrality of the molecule, with two negative and two positive charges located on the pyrophosphate group and on the base rings, respectively. This charge repartition leads to a crystal packing strongly held by electrostatic interactions between charged groups of the NAD^+ molecule. The pyrophosphate group is surrounded in the crystal by the two base rings of the NAD^+ molecule (Fig. 2) as well as by bases of symmetry-related molecules (Figs. 5, 6 and 7). Unlike the crystal structure of NAD^+Li^+, where a π–π stacking between the adenine and nicotinamide bases (d = 3.4 Å) is reported, the positive charges on both rings of the acidic form of NAD^+ is unfavourable for such an interaction. In the triclinic NAD^+ crystal, to accommodate the repulsive forces the cycles are shifted and slightly tilted, so that the negatively charged O atom of the carboxamide is intercalated between two adenine moieties related by a translation of unit-cell vector *a* (Figs. 5, 6 and 8).

The hydrogen-bond network (Table 5) contributing to the packing stability is especially dense. All water molecules in the NAD^+ crystal are involved in three or more hydrogen bonds. They are arranged in a linear way and fill the largest solvent channel of the crystal. The W3 water molecule is hydrogen bonded to W2, which itself interacts with W1. The W2 molecule is hydrogen bonded in a tetrahedral coordination (Fig. 6). As mentioned in a previous study (Guillot *et al.*, 2000), the water molecule W3 is simultaneously hydrogen bonded to both sides of the NAD^+ molecule and seems, in a striking way, to help to hold the molecule in its folded conformation (Fig. 9).

In the pyrophosphate moiety, only the O—P-type O atoms O2, O3, O8 and O9 are involved in hydrogen bonds. The three phosphoester P—O—*X* O atoms are sterically inaccessible. The case of the O3 atom is particularly noteworthy as it participates simultaneously in three hydrogen bonds (Fig. 8), which is consistent with the P1—O3 bond being on average 0.018 Å longer than the P1—O2, P2—O8 and P2—O9 bonds (Table 2). The hydrogen-bond network also leads to significant structural deformations of the NAD^+ molecule. For instance, the O2—P1—O3 angle is 115.3 (4)°, whereas the O8—P2—O9 angle is 120.3 (4)° (Table 3). One can attribute this difference to the fact that the hydrogen bonds involving the O8 and O9

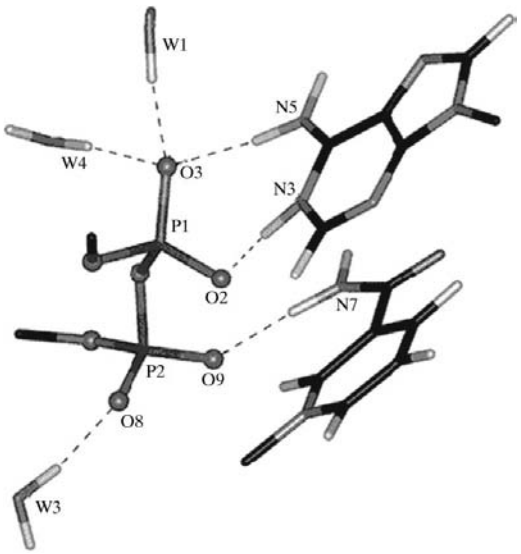

Figure 6
Hydrogen-bonding network around the pyrophosphate moiety. The pyrophosphate O atoms are displayed as spheres. For clarity, non-relevant parts of the structure have been removed from the picture.

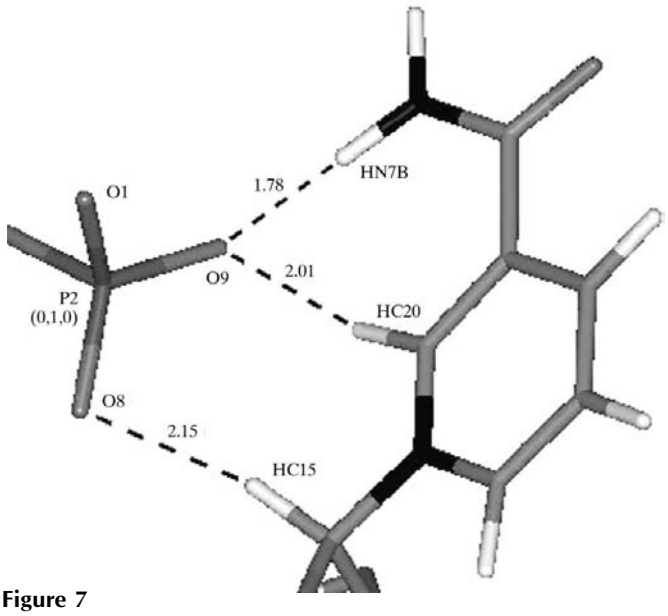

Figure 7
Intermolecular hydrogen bonds between the nicotinamide nucleoside and the pyrophosphate moiety. Interatomic distances are given in Å.

Table 6
Distances and angles of the C—H···O interactions.

C—H···O interactions	C—H (Å)	O···H (Å)	C···O (Å)	C—H···O (°)
C7—HC7···OW4^{vi}	1.101 (8)	2.025 (9)	3.095 (7)	163.1 (6)
C10—HC10···O4^{i}	1.084 (7)	2.40 (1)	3.238 (7)	132.8 (7)
C15—HC15···O8^{v}	1.108 (7)	2.148 (8)	3.233 (7)	165.4 (7)
C20—HC20···O9^{v}	1.077 (7)	2.013 (8)	3.027 (6)	155.6 (7)

Symmetry codes as in Table 5.

atoms clearly tend to pull these atoms in opposite directions, as can be seen in Fig. 8.

The amide group, which is involved in three hydrogen bonds (Table 5), is also distorted. Both H—N5 bonds deviate from the carboxamide plane by about 6° and the HN5B and HC20 atoms are only 1.98 Å apart owing to the small C20—C19—C21—N7 torsion angle (8.14°). Hence, there is an obvious ability for *a priori* rigid groups in the coenzyme to be widely deformed under external interactions and packing constraints. Moreover, the conformational variability of the NAD^+ molecule through rotations around its numerous torsion angles obviously participates in the adaptability of the NAD^+ or NADH coenzymes to bind in various enzyme active-site environments.

3.5. C—H···O interactions

There are four noteworthy short C—H···O contacts in the NAD^+ crystal structure. These interactions were located using a standard criterion based on the sum of the van der Waals radii of H and O atoms (1.1 Å for H and 1.3 Å for O); their geometrical features are listed in Table 6. The H···O distance values used in the literature vary between 2.4 and 2.8 Å (Steiner, 1996). In the present study, the cutoff for the H···O distance was set to 2.4 Å, which is a restrictive criterion allowing the avoidance of dubious long-range interactions. Interactions with a C—H···O angle lower than 120° were also disregarded. Two of the four contacts involve the adenine base and two involve the nicotinamide nucleoside. The C20—HC20···O9^{v} (Fig. 7) and C7—HC7···OW4^{vi} (Fig. 6) contacts display especially short interaction distances [d(C,O) = 3.03 and 3.09 Å, respectively] and can be considered as weak hydrogen bonds. It is also interesting to note that the C7—HC7 distance was refined to 1.101 (8) Å, which is longer than the standard value of 1.077 (12) Å for H—C sp^2 bonds (Wilson, 1995). The C15—HC15···O8^{v} (Fig. 7) and C10—HC10···O4^{i} contacts have longer characteristic distances (Table 6), the HC10···O4^{i} being at the upper limit of the selected cutoff range. Hence, the discrimination between a hydrogen bond and an electrostatic interaction is not straightforward and an analysis of the topological properties of the electron density (Bader, 1990) is needed to classify these interactions, which is the subject of a forthcoming paper.

As earlier studies have already shown the ability of adenine derivatives to frequently form such hydrogen bonds, favoured by the alternation of N and C atoms along the ring (Sutor, 1962), it is not surprising to observe several short C—H···O interactions in the NAD^+ crystal structure. Very short C7—HC7···OW4^{vi} interaction distances are usually observed in hydrogen bonds involving highly acidic C—H groups such as Cl_3CH or $(NO_2)_3CH$. Taylor & Kennart (1982), in their statistical study of C—H···*A* interactions, have shown that the presence of an N^+ atom immediately adjacent to a C—H group favours the formation of hydrogen bonds. Thus, it is likely that the protonation at the adenine N3 position raises the acidity of the C7—HC7 group, which may explain the unusual strength of the C7—HC7···OW4^{vi} hydrogen bond (Table 6).

This is consistent with the crystal structure of adenosine (Lai & Marsh, 1972), where the base is unprotonated and forms a similar C7—HC7···O hydrogen bond with a HC7···O separation of 2.4 Å, which is 0.3 Å longer than in the present NAD^+ crystal structure. Similarly, in the structure of D-glyceraldehyde-3-phosphate dehydrogenase at 1.88 Å resolution (Song *et al.*, 1999; PDB code 1dss), the NAD^+ cofactor forms C7—HC7···OD1(Asn6) hydrogen bonds with distances d(C···O) = 3.3 and 3.2 Å for the two non-crystallographic symmetry (NCS) related equivalent monomers. Interestingly, in unprotonated adenine derivatives, very short range intramolecular C10—HC10···O interactions can be found. In the case of uridylyl-(3′-5′)-adenosine monophosphate (Rubin *et al.*, 1972), the HC10···O and C10···O distances are 2.1 and 3.1 Å, respectively, suggesting that C10—H10 is probably the most acidic C—H group in neutral adenine.

The C15—HC15···O8^{v} interaction is the weakest and concerns the ribose C atom, which is adjacent to the positively charged N

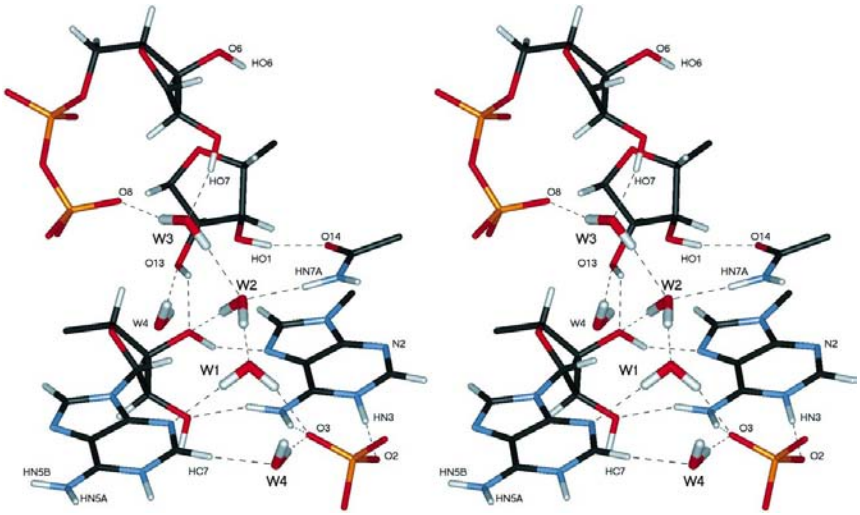

Figure 8
Hydrogen-bonding pattern around the water molecules. Only atoms involved in hydrogen bonds have been labelled. For clarity, some labels have been placed on symmetry-related groups. The water molecules have been labelled in bold.

atom N6 of the nicotinamide cycle (Fig. 7, Table 6). The C20—HC20 group of the nicotinamide cycle is hydrogen bonded to the O9^{v} pyrophosphate O atom in the NAD^{+} crystal (Fig. 7). The nicotinamide nucleoside interacts with the (x, y + 1, z) symmetry-related pyrophosphate moiety through these two C—H···O bonds and the N7—HN7B···O9^{v} hydrogen bond (Table 5, Fig. 7). Again, the C20—HC20···O9^{v} interaction distances are remarkably short and may be explained by an enhanced local acidity of the C20—HC20 group owing to the presence of electron-withdrawing groups on both sides of C20: the carboxamide group and the pyridine N1^{+} N atom. This hydrogen bond may also be strengthened by the acceptor pyrophosphate lateral O—P O atom which carries a negative charge.

However no equivalent C20—H20···O interaction was reported in either the crystal structure of the NAD^{+} lithium salt or the isolated nicotinamide moiety (Miwa *et al.*, 1999). Several occurrences of such interactions were found among the NAD^{+}–enzyme complex structures solved at resolutions better than 2 Å. For instance, in the 1.8 Å resolution crystal structure of dehydroquinate synthase (Carpenter *et al.*, 1998; PDB code 1dqs), such a hydrogen bond occurs with the OD2(Asp119) O atom, with C20···OD2 distances of 3.2 and 3.3 Å in the two holoenzymes related by NCS. In the 1dqs structure dimer, the adenine base forms an additional C—H···O interaction with distances between C17 and the Asp146 carboxylate groups of 3.2 and 3.3 Å. The 1.5 Å resolution crystal structure of phenylalanine dehydrogenase (Vanhooke *et al.*, 1999; PDB code 1bw9) displays a similarly short C20···OD1(Asn262) contact with d(C20···O) = 2.8 Å. In the 1.8 Å resolution structure of the holoenzyme UDP-galactose-4 epimerase (Thoden *et al.*, 2000; PDB code 1ek5), the nicotinamide moiety of NAD^{+} is rotated by 180° when compared with the present structure. The HC20 and HN5B atoms are then located above the ribose ring and point in the direction of the pyrophosphate to create intramolecular hydrogen bonds with the O9 atom [d(C20···O9) = 3.1 Å]. This is reminiscent of the C20—HC20···O9^{v} intermolecular interaction found in the present crystal structure. The formation of C20—HC20···O hydrogen bonds thus seems to be an inherent property of the NAD^{+} molecule and may play a role in the stereospecificity of the reactions it catalyzes.

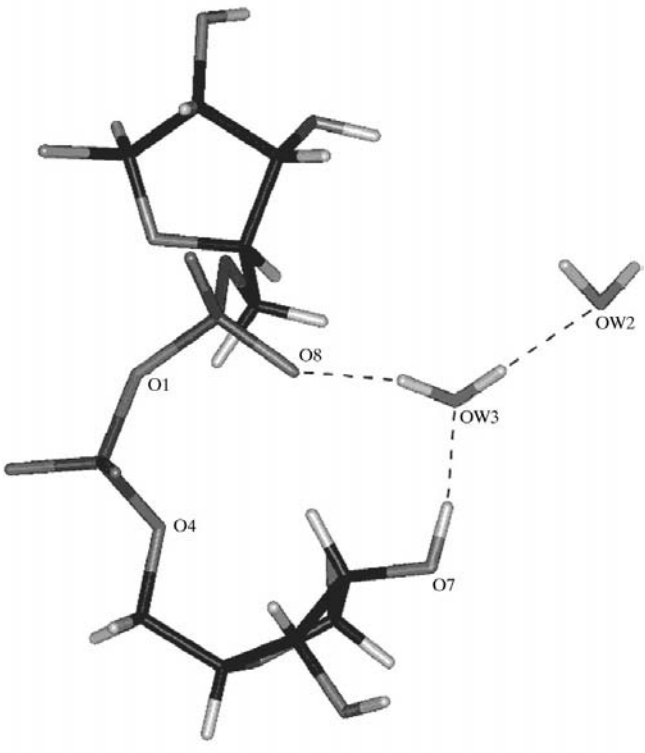

Figure 9
Intermolecular hydrogen bonding of the W3 water molecule.

References

Bader, R. F. W. (1990). *Atoms in Molecules: a Quantum Theory. The International Series of Monographs on Chemistry*, edited by J. Halpen & M. L. H. Green. Oxford: Claredon Press.

Berman, H. M., Westbrook, J., Feng, Z., Gilliland, G., Bhat, T. N., Weissig, H., Shindyalov, I. N. & Bourne, P. E. (2000). *Nucleic Acids Res.* **28**, 235–242.

Brünger, A. T. (1992). *X-PLOR Version* 3.2. *A System for X-ray Crystallography and NMR*. New York: University Press.

Burnett, M. N. & Johnson, C. K. (1996). *ORTEPIII: Oak Ridge Thermal Ellipsoid Plot Program for Crystal Structure Illustrations*. Oak Ridge National Laboratory Report ORNL-6895.

Carpenter, E. P., Hawkins, A. R., Frost, J. W. & Brown, K. A. (1998). *Nature (London)*, **394**, 299–302.

Cho, H., Ramaswamy, S. & Plapp, B. V. (1997). *Biochemistry*, **36**, 382–389.

Coppens, P. & Vos, A. (1971). *Acta Cryst.* B**27**, 146–159.

Cruickshank, D. W. J. (1999). *Acta Cryst.* D**55**, 583–601.

Dunitz, J. D. & Seiler, P. (1973). *Acta Cryst.* B**29**, 589–595.

Dunn, C. R., Banfield, M. J., Barker, J. J., Higham, C. W., Moreton, K. M., Turgut Balik, D., Brady, R. L. & Holbrook, J. J. (1996). *Nature Struct. Biol.* **3**, 911–915.

Farrugia, J. L. (1997). *J. Appl. Cryst.* **30**, 565.

Guillot, B., Jelsch, C. & Lecomte, C. (2000). *Acta Cryst.* C**56**, 726–728.

Guillot, B., Viry, L., Guillot, R., Lecomte, C. & Jelsch, C. (2001). *J. Appl. Cryst.* **34**, 214–223.

Jelsch, C., Pichon-Pesme, V., Lecomte, C. & Aubry, A. (1998). *Acta Cryst.* D**54**, 1306–1318.

Lai, T. F. & Marsh, R. E. (1972). *Acta Cryst.* B**28**, 1982–1988.

Hansen, N. K. & Coppens, P. (1978). *Acta Cryst.* A**34**, 909–921.

Hirshfeld, F. L. (1976). *Acta Cryst.* A**32**, 239–244.

Miwa, Y., Mizuno, T., Tsushida, K., Taga, T. & Iwata, Y. (1999). *Acta Cryst.* B**55**, 78–84.

Mullichak, A. M., Theisen, M. J., Essigmann, B., Benning, C. & Garavito, R. M. (1999). *Proc. Natl. Acad. Sci. USA*, **96,** 13097–13102.

Parthasarathy, R. & Fridey, S. M. (1984*a*). *Am. Cryst. Assoc. Ser. 2*, **12**, 54.

Parthasarathy, R. & Fridey, S. M. (1984*b*). *Science*, **226**, 969–971.

Reddy, B. S., Saenger, W., Mühllegger, K. & Weimann, G. (1981). *J. Am. Chem. Soc.* **103**, 907–914.

Rubin, J., Brennan, T. & Sundaralingam, M. (1972). *Biochemistry*, **11**, 3112–3128.

Saenger, W., Reddy, B. S., Mühllegger, K. & Weimann, G. (1977). *Nature (London)*, **267**, 225–229.

Song, S. Y., Xu, Y. B., Lin, Z. J. & Tsou, C. L. (1999). *J. Mol. Biol.* **287**(4), 719–25.

Steiner, T. (1996). *Cryst. Rev.* **6**, 1–57.

Sutor, D. J. (1962). *Nature (London)*, **195**, 68–69.

Taylor, R. & Kennart, O. (1982). *J. Am. Chem. Soc.* **104**, 5063–5070.
Thoden, J. B., Gulick, A. M. & Holden, H. M. (1997). *Biochemistry*, **36**(35), 10685–10695.
Thoden, J. B., Hegeman, A. D., Wesenberg, G., Chapeau, M. C., Frey, P. A. & Holden, H. M. (1997). *Biochemistry*, **36**(21), 6294–6304.
Thoden, J. B., Wohlers, T. M., Fridovich-Keil, J. L. & Holden, H. M. (2000). *Biochemistry*, **39**, 5691–5701.
Vanhooke, J. L., Thoden, J. B., Brunhuber, N. M., Blanchard, J. S. & Holden, H. M. (1999). *Biochemistry*, **38**, 2326–2339.
Wilson, A. J. C. (1995). *International Tables for Crystallography*, Vol. C. Dordrecht: Kluwer Academic Press.